

17. We prepared the PPV by using a modified version of the Wessling route [R. A. Wessling and R. G. Zimmerman, U.S. Patent 3,401,152 (1968); U.S. Patent 3,706,677 (1972)] as described by F. Papadimitrakopoulos *et al.* [*Chem. Mater.* **6**, 1563 (1994)].
18. We measured the internal quantum efficiencies by placing the LED directly on the Si photodiode and measuring the photocurrent (I_{ph}) as a function of the forward current (I_f). The ratio I_{ph}/I_f was multiplied by 700 to obtain the values.
19. M. Yan, L. J. Rotheberg, F. Papadimitrakopoulos, M. E. Galvin, T. M. Miller, *Phys. Rev. Lett.* **72**, 1104 (1994).
20. Changing substituents on the phenyl groups has only a very small effect on the reduction potentials (for example, compare **11** and **12**).
21. S. M. Sze, *Semiconductor Devices, Physics and Technology* (Wiley, New York, 1985).
22. Devices were stored in an Ar-filled dry box.
23. For example, poly(aryl ether quinoxaline)s and poly(aryl ether pyridyltriazine)s. M. Strukelj, J. Hamier, E. Elce, A. S. Hay, *J. Polym. Sci. Polym. Chem. Ed.* **32**, 193 (1994); M. Strukelj and J. C. Hedrick, *Macromolecules* **27**, 7511 (1994).
24. The current was increased from 0 to 50 mA in 200- μ A increments over \sim 90 s.
25. F. Garnier *et al.*, *J. Am. Chem. Soc.* **115**, 8716 (1993); F. Garnier, R. Hajlaoui A. Yassar, P. Srivastava, *Science* **265**, 1684 (1994).
26. The work of M.S. was supported under a Natural Sciences and Engineering Council of Canada post-doctoral fellowship. Useful comments on the manuscript by E. A. Chandross, H. Katz, A. Dodabalapur, and M. Galvin are appreciated.

26 October 1994; accepted 25 January 1995

High-Pressure Elasticity of Iron and Anisotropy of Earth's Inner Core

Lars Stixrude*† and R. E. Cohen

A first principles theoretical approach shows that, at the density of the inner core, both hexagonal [hexagonal close-packed (hcp)] and cubic [face-centered-cubic (fcc)] phases of iron are substantially elastically anisotropic. A forward model of the inner core based on the predicted elastic constants and the assumption that the inner core consists of a nearly perfectly aligned aggregate of hcp crystals shows good agreement with seismic travel time anomalies that have been attributed to inner core anisotropy. A cylindrically averaged aggregate of fcc crystals disagrees with the seismic observations.

There is a growing body of seismic evidence that Earth's inner core, a 1200-km solid iron-alloy sphere at the center of our planet, is elastically anisotropic. This observation promises to shed new light on a number of geophysical problems including the crystalline structure of the inner core, its formation by the freezing of the overlying outer core (a process that is thought to be a major energy source driving the fluid motions that produce the geomagnetic field), and the influence of the inner core on the geometry of the geomagnetic field itself.

The seismological data consist of the anomalous splitting of free oscillation frequencies (1, 2) and travel time observations (3–9), which show that compressional waves that traverse the inner core (PKIKP) travel 3 to 4% faster along Earth's spin axis than in the equatorial plane. Most studies agree that the data can be accounted for in terms of cylindrically symmetric elastic anisotropy in the inner core nearly aligned with Earth's spin axis. In detail, inversions of the data are inherently nonunique, and there are important

differences among models regarding the magnitude of the anisotropy, its depth dependence, and its degree of alignment with the spin axis. In particular, models based on free oscillation data and those based on travel time observations have been mutually inconsistent. These inconsistencies have led to some doubt about whether the inner core is the source of the anomalous observations (10). A recent model (2) has been shown to underestimate substantially travel time anomalies along near-antipodal paths (8, 11). These inconsistencies, together with our lack of knowledge of the elastic properties of solid iron at inner core pressures (330 to 360 GPa) and temperatures (4000 to 8000 K), have made the seismological observations difficult to interpret in terms of physical models of the origin of inner core anisotropy (12, 13).

Here we investigate whether the physical properties of iron are consistent with anisotropy in Earth's inner core. We describe forward models of the inner core based on predictions of the elasticity of iron at high pressure from solid-state theoretical methods. Our approach, which is independent of seismological data, is able to explain a large part of the travel time observations and provides substantial support for the hypothesis of inner core anisotropy.

We assume, in accord with previous work, that the inner core is composed of

nearly pure iron (14, 15) and that the seismically observed anisotropy is the result of intrinsic crystalline anisotropy. The latter assumption is natural because all known phases of iron either are strongly elastically anisotropic at ambient pressure or are likely to be so on the basis of analog compounds (16–18). The stable phase of iron at inner core conditions is unknown. Of the known phases of iron, we consider face-centered-cubic (fcc) and hexagonal close-packed (hcp) but not body-centered-cubic (bcc) as this phase is elastically unstable at high pressure and is thus not expected to exist in the inner core (19).

Our calculations are based on a Slater-Koster total energy, tight-binding Hamiltonian (20, 21). The parameters of the Hamiltonian are fitted to the most accurate band structures and total energies of fcc, hcp, and bcc phases available from full-potential, linearized augmented plane wave (LAPW) calculations in the generalized gradient approximation performed over a range of volumes that span Earth's pressure regime (19). The LAPW calculations are parameter-free and are completely independent of experimental data. With the tight-binding Hamiltonian, we are able to compute properties orders of magnitude faster than with the LAPW method but with no significant loss of accuracy.

We determined the single-crystal, elastic-constant tensor, C_{ijkl} , of each phase at the seismologically observed density of the inner core (22) by calculating total energies with the Slater-Koster Hamiltonian as a function of high-symmetry lattice strains (23). We fully account for coupling of the elastic constants in hcp to zone-center vibrational modes. The calculated elastic constants (Table 1) completely determine the single-crystal elastic wave velocities for

Table 1. Elastic properties of single-crystal fcc and hcp iron ($\rho = 13 \text{ Mg/m}^3$), a cylindrically averaged fcc aggregate [$(fcc)_{cyl}$ (see text)], and at the surface of a recent, depth-dependent inverse model of the inner core. Normal mode observations constrain three combinations of elastic constants: $\alpha = (C_{33} - C_{11})/A_0$, $\beta = (C_{44} - C_{66})/A_0$, and $\gamma = (C_{12} - C_{13})/A_0$, where $A_0 = \rho V_{P0}^2$; α , β , and γ determine the anisotropy of P , S_{eq} , and S_{me} waves, respectively (2, 29).

Parameter	fcc	hcp	$(fcc)_{cyl}$	Inner core (2)
C_{11} (GPa)	1658	1801	1936	
C_{12}	941	865	848	
C_{44}	636	445	451	
C_{33}		1919	2028	
C_{13}		810	1206	
α (%)		+6.5	+4.9	+6.8
β		-1.3	-4.9	-0.9
γ		+3.1	-19.1	-2.3
$\varepsilon = (\alpha - 4\beta + 2\gamma)/4$		+4.5	-3.4	+1.5

*L. Stixrude, Institut für Geophysik, Universität Gottingen, 37075 Gottingen, Germany.

R. E. Cohen, Geophysical Laboratory and Center for High Pressure Research, Carnegie Institution of Washington, Washington, DC 20015, USA.

*On leave from the School of Earth and Atmospheric Sciences, Georgia Institute of Technology, Atlanta, GA 30332, USA.

†To whom correspondence should be addressed.

propagation direction, \mathbf{n} , and polarization vector, \mathbf{w} (24),

$$\rho V^2 = \sum_{i,j,k,l=1}^3 w_i n_j w_k n_l C_{ijkl} \quad (1)$$

where V is the velocity and ρ is the density. We find (Fig. 1) that both fcc and hcp are substantially anisotropic in compressional (P) and shear (S) wave velocities. The magnitude of the anisotropy is much greater in the cubic phase (25), but either structure is sufficiently anisotropic to account for the seismic observations (the anisotropy of a polycrystalline aggregate must be less than or equal to that of a single crystal).

To apply our single-crystal results, we require a model of polycrystalline texture in the inner core. In the absence of independent information, we take the simplest possible forms that are consistent with cylindrical symmetry. For hcp, we take an aggregate with all [001] axes aligned with Earth's spin axis. The effective elastic constants of an

inner core composed of such an aggregate are identical to those of the hcp single crystal. For fcc, we take an aggregate with all [111] axes aligned with Earth's spin axis but otherwise randomly oriented. The effective elastic constants of this cylindrically averaged fcc aggregate are calculated from the single-crystal fcc elastic constants (Table 1).

In the case of cylindrical symmetry and P -wave propagation, appropriate for comparison with travel time observations, Eq. 1 reduces to

$$\rho V_p^2(\xi) = C_{11} + (4C_{44} + 2C_{13} - 2C_{11})\cos^2(\xi) + (C_{33} + C_{11} - 4C_{44} - 2C_{13})\cos^4(\xi) \quad (2)$$

where the C_{ij} values are given in Table 1 and ξ is the angle between the inner core segment of PKIKP and the rotation axis. Equivalent expressions have been given by others (2-4, 7). We approximate PKIKP travel-time anomalies due to inner core anisotropy by

$$\delta t(\Delta, \xi) = -t(\Delta)\delta V_p(\xi)/V_{P0} \quad (3)$$

where Δ is the angular distance from source to receiver, t is the travel time of the PKIKP wave in the inner core, and the velocity anomaly is given by $\delta V_p(\xi) = V_p(\xi) - V_{P0}$, where V_{P0} is the Voight-Reuss-Hill average velocity (3, 26). We considered two distance ranges corresponding to recent determinations of travel time differences between PKP_{BC} and PKIKP phases (BC - DF), and PKP_{AB} and PKIKP phases (AB - DF) (27).

The hcp forward model of inner core anisotropy is in good agreement with BC - DF travel time observations, particularly those near the pole and near the equator (Fig. 2). The magnitude of the polar (+4 s) and equatorial (< +1 s) travel time anom-

alies are well reproduced. Like most inversions of seismic data, we predict an off-axis minimum in the travel time anomaly and a region of slow arrivals relative to equatorial paths. The magnitude of the minimum (centered at $\xi = 56^\circ$) is overestimated. Nevertheless, our results yield a variance reduction of the observations (3, 7) of 53% and a root mean square error of 0.08 s, compared with 90% and 0.06 s, respectively, for a best fit to the data (7). The anomalous AB - DF observations of (8) are clustered near $\xi = 29^\circ$. For these ray paths, we predict a travel time anomaly due to inner core anisotropy of 3.5 s, consistent with the range of observed values (3.0 to 6.1 s) (28).

Our hcp forward model predicts equatorially (S_{eq}) and meridionally (S_{me}) polarized S -wave anisotropies that have the same sense as that determined at the surface of the inner core in at least one inversion (2, 29). Both forward and inverse models predict S_{eq} waves that are slow along the spin axis relative to the equatorial plane and S_{me} -wave velocities that are fastest for $\xi = 45^\circ$ (Table 1). In the case of S_{eq} waves, the magnitude of the anisotropy is also similar in forward and inverse models. The S -wave anisotropy of the inner core is comparatively poorly known seismologically; as it is constrained by the anomalous splitting of only a few free oscillation frequencies. Other inversions, based only on free oscillations, have determined S_{eq} -wave anisotropies of the opposite sense to those in our model (S_{eq} waves that are fast along the spin axis). The PKJKP (30) travel times may best constrain the S -wave anisotropy of the inner core, but this phase has not yet been observed. Our hcp model predicts a large S_{me} - S_{eq} splitting of this phase, with S_{me} waves arriving as much as

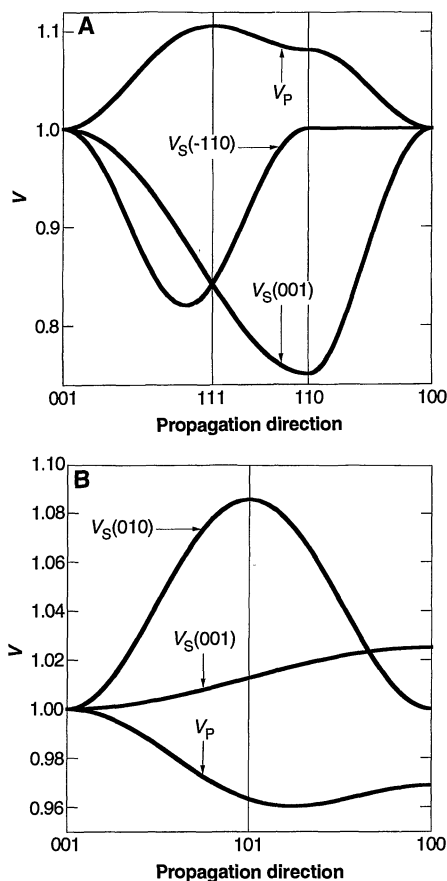


Fig. 1. Single-crystal velocities in fcc (A) and hcp (B) iron at a density of $\rho = 13 \text{ Mg/m}^3$. Planes of polarization are indicated for S waves. Velocities are normalized to those corresponding to propagation along [001], for which shear-wave velocities are degenerate in both crystals. For fcc, velocities along [001] (in kilometers per second) are 11.28 (V_p) and 6.98 (V_s); for hcp, 12.13 (V_p) and 5.84 (V_s).

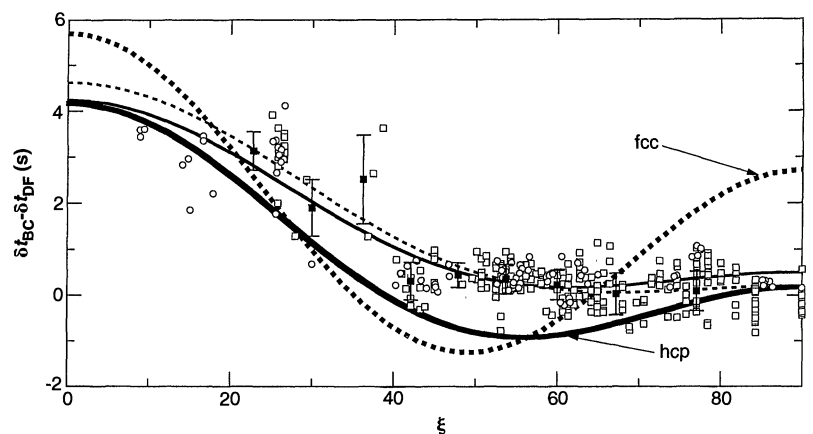


Fig. 2. Plot of BC - DF travel time anomalies as a function of the angle ξ between the inner core ray segment and Earth's spin axis for $\Delta = 150^\circ$ (see text). The forward models described in the text for an inner core consisting of an hcp aggregate (bold solid line) and a cylindrically averaged fcc aggregate (bold dashed line) are compared with observations and the best fits to the two data sets [circles and thin solid line (7), squares and thin dashed line (3)]. The binned data of (3) are also shown (solid squares with error bars).

50 s earlier than S_{eq} waves (31). If this prediction is verified, the inner core would be the source of the largest shear-wave splitting in Earth.

The fcc aggregate yields much poorer agreement with observations (Fig. 2). Travel time anomalies at the pole (+5.8 s) and equator (+2.8 s) are overestimated, and the region of anomalously slow travel times is more pronounced than in the case of the hcp aggregate. The variance reduction of the BC – DF data (3, 7) is only 19%. The S_{eq} -wave anisotropies are predicted to have the same sense as the surface of the inverse model (2), but S_{me} -wave anisotropy has the opposite sense. These results are consistent with earlier work (32) in which symmetry arguments were used to show that aggregates of cubic crystals, regardless of their texture, would yield poor agreement with seismic data.

The differences between the hcp forward model and the details of the observed angular dependence of BC – DF anomalies have several possible sources. First, our simple models of texturing are not likely to be correct in detail. A more complex texture in which the degree of alignment depends on ξ will produce better agreement with the seismic data. Our elastic constants could be used to derive a texture that best fits the observations (33). Second, we have not considered a cylindrical symmetry axis that is tilted with respect to the spin axis, or more general, small, noncylindrical contributions to the anisotropy that are indicated by some inversions (3, 9). Third, small amounts of alloying constituents that likely exist in the inner core may effect its elastic anisotropy (34). Fourth, the elastic anisotropy of iron may be affected by the temperature difference between our athermal (0 K) calculations and the inner core. Finally, theoretical errors must be considered, because of the approximate exchange correlation potentials upon which the LAPW calculations are based, or because of approximations in the tight-binding model.

The level of agreement between first principles theory and seismological observation is encouraging and supports the hypothesis that the P -wave travel time anomalies are caused by elastic anisotropy in the inner core and that this region is composed of hcp iron. The assumed textures are the simplest possible and suggest that the inner core may be much more strongly textured than previously thought. The degree of texturing required by our results is much greater than that predicted for a convecting inner core by Wenk *et al.* (18). Their study indicated a sixfold reduction, relative to the single crystal value, of the anisotropy of an aggregate subject to a convection-induced strain field, which would correspond to P -wave anisotropies no larger than 0.2%.

However, substantially larger strains than those assumed or different convection geometries may be able to produce the required bulk anisotropy (18). The efficiency of the magnetic alignment mechanism, whereby induced magnetic moments are aligned with the geomagnetic field (13), is unknown and will depend critically on the unknown magnetic susceptibility of hcp iron. Magnetic properties are an important issue for another reason. The strong textures indicated by our work suggest that the bulk magnetic susceptibility of the inner core may be significantly anisotropic. This may have important implications for the influence of the inner core on the geometry of the geomagnetic field (35).

In addition to the texturing mechanisms already proposed, the stress induced by the rotation of the inner core may play an important role in producing lattice-preferred orientation. The nonhydrostatic stress field induced by rotation is such that the magnitude of the principal stress parallel to the spin axis is everywhere twice that in either of the equatorial directions. The hcp texture we assumed is the equilibrium configuration under this stress field because it minimizes the induced elastic strain energy. The strain energy is minimized by aligning the direction of stiffest elastic response of the constituent crystals, corresponding to the direction of maximum P -wave velocity [001], with the spin axis. For the high temperatures and long time scales available, we speculate that the inner core may be able to recrystallize in the solid state such that it attains this minimum energy texture (36). The magnitude of the stress field would be increased by other zonally dependent processes, such as a zonally dependent crystallization rate of the inner core, which has also been proposed as the origin of inner core anisotropy (37).

The hcp textural model assumed here is elastically indistinguishable from a single crystal. The very strong texturing indicated by our results suggests the possibility that the inner core is a very large single crystal. The high temperatures and slow growth rate of the inner core, compared with the temperatures and growth rates encountered in igneous and hydrothermal contexts, may prove ideal for growing single crystals much larger than those observed in the near-surface environment.

REFERENCES AND NOTES

1. J. H. Woodhouse, D. Giardini, X. D. Li, *Geophys. Res. Lett.* **13**, 1549 (1986).
2. J. Tromp, *Nature* **366**, 678 (1993).
3. K. C. Creager, *ibid.* **356**, 309 (1992).
4. A. Morelli, A. M. Dziewonski, J. H. Woodhouse, *Geophys. Res. Lett.* **13**, 1545 (1986).
5. P. M. Shearer, K. M. Toy, J. A. Orcutt, *Nature* **333**, 228 (1988).
6. P. M. Shearer and K. M. Toy, *J. Geophys. Res.* **96**, 2233 (1991).
7. X. Song and D. V. Helmberger, *Geophys. Res. Lett.* **20**, 2233 (1993).
8. L. Vinnick, B. Romanowicz, L. Breger, *ibid.* **21**, 1671 (1994).
9. W. J. Su and A. M. Dziewonski, *Seismol. Res. Lett.* **65**, 23 (1994).
10. R. Widmer, T. G. Masters, F. Gilbert, *Geophys. J. Int.* **111**, 559 (1992).
11. Inversions based on normal modes generally assume a depth-dependent anisotropy that decays smoothly to zero at the center of the inner core. This assumption, which is made because normal mode frequencies are insensitive to anisotropy deep in the inner core, may be the source of the discrepancy with travel time observations. Joint inversions of normal mode and travel time data may resolve these discrepancies.
12. R. Jeanloz and H. R. Wenk, *Geophys. Res. Lett.* **15**, 72 (1988).
13. S.-I. Karato, *Science* **262**, 1708 (1993).
14. A. P. Jephcoat and P. L. Olson, *Nature* **325**, 332 (1987).
15. H. K. Mao, Y. Wu, L. C. Chen, J. F. Shu, A. P. Jephcoat, *J. Geophys. Res.* **95**, 21737 (1990).
16. M. W. Guinan and D. N. Beshers, *J. Phys. Chem. Solids* **29**, 541 (1968).
17. J. Zaretsky and C. Stassis, *Phys. Rev. B* **35**, 4500 (1987).
18. H. R. Wenk, T. Takeshita, R. Jeanloz, G. C. Johnson, *Geophys. Res. Lett.* **15**, 76 (1988).
19. L. Stixrude, R. E. Cohen, D. J. Singh, *Phys. Rev. B* **50**, 6442 (1994).
20. R. E. Cohen, M. J. Mehl, D. A. Papaconstantopoulos, *ibid.*, p. 14694. The two-center, nonorthogonal Slater-Koster tight-binding Hamiltonian includes all s , p , and d interactions and eliminates the essential ambiguity of the energy zero, V_0 , of non-self-consistent treatments. The quantity V_0 is set such that the total energy is given simply as a sum over the bands; that is, there is no pair-potential or other non-band-structure term. This parametrization reproduces LAPW total energies and band structures of iron with a root mean square error of 0.5 and 5 mRy, respectively. The most important physical assumption on which our calculations are based is the generalized gradient approximation [J. P. Perdew *et al.*, *Phys. Rev. B* **46**, 6671 (1992)] to the exchange-correlation terms, which is the only approximation made in the LAPW calculations. For a general discussion of the tight-binding method, see W. A. Harrison, *Electronic Structure and the Properties of Solids* (Freeman, San Francisco, 1980).
21. R. E. Cohen, L. Stixrude, D. A. Papaconstantopoulos, in *High Pressure Science and Technology—1993*, S. C. Schmidt, J. W. Shaner, G. A. Samara, M. Ross, Eds. (American Institute of Physics, New York, 1994), pp. 891–894.
22. T. G. Masters and P. M. Shearer, *J. Geophys. Res.* **95**, 21691 (1990). The uncertainty in the seismologically determined inner core density and its slight increase with depth (both several percent) are unimportant for our study because they are much smaller than the relative uncertainty in the travel time anomalies due to anisotropy.
23. M. J. Mehl, J. E. Osburn, D. A. Papaconstantopoulos, and B. M. Klein [*Phys. Rev. B* **41**, 10311 (1990)] discuss the calculation of elastic constants from total energy methods.
24. D. C. Wallace, *Thermodynamics of Crystals* (Wiley, New York, 1972).
25. The greater anisotropy of the cubic phase, the relative magnitudes of P - and S -wave anisotropies, and the extremum directions of P - and S -wave velocities in both phases are consistent with ambient pressure measurements of other hcp transition metals with similar c/a ratios and fcc transition metals [E. A. Brandes, Ed., *Smithells Metals Reference Book* (Butterworths, London, 1983)] and with a nearest neighbor central-force model [M. Born and K. Huang, *Dynamical Theory of Crystal Lattices* (Oxford Univ. Press, Oxford, 1954), pp. 140–149]. The magnitude of P -wave anisotropy in hcp iron predicted here is in excellent agreement with the systematic-based estimate of Wenk *et al.* (18).

26. These are 11.92 km/s for fcc and 11.73 km/s for hcp.
27. We focus on differential travel times because these are least contaminated by other potential sources of velocity anisotropy. The abbreviations PKP_{BC} and PKP_{AB} refer to ray paths that are shallower than $PKIKP$ so that they do not enter the inner core; PKP_{DF} is synonymous with $PKIKP$. Anomalous BC – DF (3, 7) observations are centered near $\Delta = 150^\circ$ ($t = 124$ s); anomalous AB – DF observations (8) are clustered near $\Delta = 175^\circ$ ($t = 230$ s). To ensure an even coverage in ξ for both BC – DF data sets, we used the binned data of Creager (3). The BC – DF and AB – DF travel times are corrected for the ellipticity of Earth.
28. The AB – DF travel times are likely biased by mantle structure so that they are larger (by approximately 0.5 s) than what inner core structure alone would produce (8).
29. S_{ec} is polarized in the equatorial plane, S_{me} in the meridional plane defined by the propagation direction and the rotation axis. In the hcp forward model of the inner core, these polarizations correspond to the (001) and (010) crystallographic planes, respectively.
30. This is a converted phase that travels as an S wave only in the inner core.
31. The S_{ec} and S_{me} travel times were computed for $\xi = 45^\circ$ and $\Delta = 260^\circ$ in the IASP91 model [B. N. L. Kennett and E. R. Engdahl, *Geophys. J. Int.* **105**, 429 (1991)] with a code provided by C. W. Wicks.
32. C. M. Sayers, *Geophys. J. Int.* **103**, 285 (1990).
33. ———, *Geophys. Res. Lett.* **16**, 267 (1989).
34. The effect of nickel, which is thought to be the most abundant alloying constituent, is probably small. The equation of state of iron-nickel alloys at core pressures is known to be virtually independent of composition up to 20% nickel (15). The light element that is present in the outer core (possibly O, S, Si, H, or C) may exist in the inner core as well. The effect of this light element is expected to be small because seismological observations constrain its abundance in the inner core to less than a few percent (14).
35. R. Hollerbach and C. A. Jones, *Nature* **365**, 541 (1993).
36. Paleomagnetic data indicate that the inner core was formed at least 4 billion years ago. If we assume a

- linear growth rate, the outermost 300 km, to which the BC – DF observations are most sensitive, would have formed in 1 billion years. Recent observations, which indicate that the outermost 50 to 100 km of the outer core is isotropic [X. Song and D. V. Helmberger, *J. Geophys. Res.*, in press; P. Shearer, *ibid.* **99**, 19647 (1994)], suggest that these most recently formed regions may not have had sufficient time to develop anisotropy through recrystallization.
37. This mechanism is discussed in F. D. Stacey, *Physics of the Earth* (Brookfield, Auckland, New Zealand, 1992), pp. 210–211.
38. We thank K. Creager (3) and X. Song (7) for providing their travel time data in digital form, C. W. Wicks for the code used to calculate $PKIKP$ travel times, and U. Christensen, R. Jeanloz, P. Shearer, X. Song, J. Tromp, and C. Wicks for comments on the manuscript and helpful discussions. Supported by the National Science Foundation under grant EAS-9305060. L.P.S. was also supported by an Alexander von Humboldt Foundation fellowship.

9 November 1994; accepted 19 January 1995

Biogeological Mineralization in Deep-Sea Hydrothermal Deposits

Terri L. Cook* and Debra S. Stakes

Oriented drill cores retrieved from active massive sulfide edifices at the Endeavour Segment of the Juan de Fuca Ridge contain an abundance of fossilized tube structures associated with vestimentiferan and annelid worms. The petrological evolution of these biogeological structures and their presence deep inside the edifice walls demonstrate that an initial, worm-mediated texture directly affects the subsequent steps of inorganic precipitation, wall infilling, and outward growth of these black smoker deposits. The presence of fossilized structures in hydrothermal discharge sites that are 2 kilometers apart and their similarity to structures observed in other modern and ancient deposits suggest that these biogeological processes are general phenomena.

Although the presence of biological structures or their remains in northeast Pacific mid-ocean ridge sulfide deposits has been commonly reported (1–7), an understanding of both the biogeological interactions and the processes of hydrothermal mineralization has been difficult to obtain because of a lack of oriented samples encompassing the outward growth of the deposits. Here we describe worm-derived textures in oriented cores drilled into the main bodies of large black smoker edifices (4, 8). These textures are composed of distinctive, concentrically layered worm tube structures generally surrounded by massive, wall-infilling crystals. Similar tube structures have been described as cross sections of fossilized chitinous worm tubes (6), and the concentric mineralogical layering has been observed in many sulfide deposits (2–6, 9, 10). Five petrological se-

quences observed in the drill cores show that the development of this concentric layering is initiated by the presence of worms and may also be controlled by microflora before inorganic reactions dominate the final stages of its development. Preservation of the tube structures after abandonment or decay of the organic matter provides ample fluid conduits that influence the edifices' thermal and chemical gradients and porosity (5, 11), directly affecting lateral growth.

The Endeavour sulfide zone encompasses two major active hydrothermal areas: the High Rise Site (HRS) (8) and the Main Field Site (MFS) (2, 12) (Fig. 1). The largest, northernmost structures in both fields are characterized by four venting types: small (i) black and (ii) white smoker chimneys atop the edifices, (iii) high-temperature fluids pooled beneath protruding, ledge-type "flanges," and (iv) diffuse flow through the flanges (8, 12).

We focus on three drill cores collected in 1991. All three were drilled from active edifices (4), although the sampled areas were inactive and biologically barren. (i) Core 2466 was drilled from the base of the

Hulk edifice in the northern MFS (12) (Fig. 1). The core is divided into six pieces totaling 27 cm in length and is composed of massive Fe and Zn sulfides (Table 1). Tube structures are present throughout the core and are associated with barite in pieces A and B. (ii) Core 2464 was drilled from Godzilla, an edifice in the northernmost HRS (Fig. 1). The core was drilled into a flange scar (flange attachment point characterized by remnant horizontal layering) halfway up the 45-m-high structure (8). Core 2464 is divided into seven pieces totaling 30 cm. The dominant mineral phase varies between pieces in this core, which is unusual for samples in this study (Table 1). Numerous fossilized tube structures up to 1 cm wide are observed in all but the innermost piece. The structures are associated with barite in piece A. (iii) Core 2461 is from the base of Boardwalk, another large structure at the northern HRS (8). This core is divided into seven pieces totaling 29 cm and is dominantly composed of Fe and Zn sulfides and amorphous silica (Table 1). Barite is present throughout the core and is associated with abundant tube structures in the interior end and center.

Our criteria for the identification of worm tube structures are based on examples from modern and ancient deposits (1–6, 9, 10). Most Endeavour sulfide samples contain large numbers of living alvinellid polychaete and vestimentiferan worms, which occupy up to 25% of the total sample volume. Poorly consolidated chimney material commonly fell apart when the worms were removed. The oval layering that we describe as worm tube structures is the only space in the outer sulfide wall that can accommodate the abundance of living worms covering the active edifices (12–14).

The textures of the tube structures and commonly their mineralogy differ from those of the wall matrix material. Most thin sections contain 20 to 35% tube structures,

T. L. Cook, Monterey Bay Aquarium Research Institute, 160 Central Avenue, Pacific Grove, CA 93950, and Earth Sciences Board, University of California, Santa Cruz, CA 95064, USA.

D. S. Stakes, Monterey Bay Aquarium Research Institute, 160 Central Avenue, Pacific Grove, CA 93950, USA.

*To whom correspondence should be addressed at the Monterey Bay Aquarium Research Institute.